Beam–Beam Effects

W. Herr and T. Pieloni
CERN, Geneva, Switzerland

Abstract
One of the most severe limitations in high-intensity particle colliders is the beam–beam interaction, i.e. the perturbation of the beams as they cross the opposing beams. This introduction to beam–beam effects concentrates on a description of the phenomena that are present in modern colliding beam facilities.

arXiv:1601.05235v1 [physics.acc-ph] 20 Jan 2016

1 Introduction

The problem of the beam–beam interaction is the subject of many studies since the introduction of the first particle colliders. It has been and will be one of the most important limits to the performance and therefore attracts interest at the design stage of a new colliding beam facility. A particle beam is a collection of a large number of charges and represents an electromagnetic potential for other charges. It will therefore exert forces on itself and other beams. The forces are most important for high-density beams, i.e. high intensities and small beam sizes, which are the key to high luminosity.

The electromagnetic forces from particle beams are very non-linear and result in a wide spectrum of consequences for the beam dynamics. Furthermore, as a result of the interaction, the charge distribution creating the disturbing fields can change as well. This has to be taken into account in the evaluation of beam–beam effects and in general a self-consistent treatment is required.

Although we now have a good qualitative understanding of the various phenomena, a complete theory does not exist and exact predictions are still difficult. Numerical techniques such as computer simulations have been used with great success to improve the picture on some aspects of the beam–beam interaction while for other problems the available models are not fully satisfactory in their predictive power.

2 Beam–beam force

In the rest frame of a beam we have only electrostatic fields and, to find the forces on other moving charges, we have to transform the fields into the moving frame and to calculate the Lorentz forces (see [1] to [5] and references therein).

The fields are obtained by integrating over the charge distributions. The forces can be defocusing or focusing, since the test particle can have the same or opposite charge with respect to the beam producing the forces.

The distribution of particles producing the fields can follow various functions, leading to different fields and forces. It is not always possible to integrate the distribution to arrive at an analytical expression for the forces, in which case either an approximation or numerical methods have to be used. This is in particular true for hadron beams, which usually do not experience significant synchrotron radiation and damping. For e^-e^+ colliders the distribution functions are most likely Gaussian with truncated tails.

In the two-dimensional case of a beam with bi-Gaussian beam density distributions in the transverse planes, i.e. $\rho(x,y) = \rho_x(x) \cdot \rho_y(y)$ with r.m.s. of σ_x and σ_y,

$$\rho_u(u) = \frac{1}{\sigma_u\sqrt{2\pi}} \exp\left(-\frac{u^2}{2\sigma_u^2}\right), \text{ where } u = x, y, \tag{1}$$

one can give the two-dimensional potential $U(x, y, \sigma_x, \sigma_y)$ as a closed expression:

$$U(x, y, \sigma_x, \sigma_y) = \frac{ne}{4\pi\epsilon_0} \int_0^\infty \frac{\exp(-\frac{x^2}{2\sigma_x^2+q} - \frac{y^2}{2\sigma_y^2+q})}{\sqrt{(2\sigma_x^2+q)(2\sigma_y^2+q)}} \mathrm{d}q, \tag{2}$$

where n is the line density of particles in the beam, e the elementary charge and ϵ_0 the permittivity of free space [6]. From the potential one can derive the transverse fields $\vec{E}$ by taking the gradient $\vec{E} = -\nabla U(x, y, \sigma_x, \sigma_y)$.

3 Elliptical beams

For the above case of bi-Gaussian distributions (i.e. elliptical beams with $\sigma_x \neq \sigma_y$) the fields can be derived and, for the case of $\sigma_x > \sigma_y$, we have [7]

$$E_x = \frac{ne}{2\epsilon_0\sqrt{2\pi(\sigma_x^2 - \sigma_y^2)}} \mathrm{Im}\left[\mathrm{erf}\left(\frac{x + \mathrm{i}y}{\sqrt{2(\sigma_x^2 - \sigma_y^2)}}\right) - \mathrm{e}^{\left(-\frac{x^2}{2\sigma_x^2} + \frac{y^2}{2\sigma_y^2}\right)} \mathrm{erf}\left(\frac{x\frac{\sigma_y}{\sigma_x} + \mathrm{i}y\frac{\sigma_x}{\sigma_y}}{\sqrt{2(\sigma_x^2 - \sigma_y^2)}}\right)\right], \tag{3}$$

$$E_y = \frac{ne}{2\epsilon_0\sqrt{2\pi(\sigma_x^2 - \sigma_y^2)}} \mathrm{Re}\left[\mathrm{erf}\left(\frac{x + \mathrm{i}y}{\sqrt{2(\sigma_x^2 - \sigma_y^2)}}\right) - \mathrm{e}^{\left(-\frac{x^2}{2\sigma_x^2} + \frac{y^2}{2\sigma_y^2}\right)} \mathrm{erf}\left(\frac{x\frac{\sigma_y}{\sigma_x} + \mathrm{i}y\frac{\sigma_x}{\sigma_y}}{\sqrt{2(\sigma_x^2 - \sigma_y^2)}}\right)\right]. \tag{4}$$

The function erf(t) is the complex error function

$$\mathrm{erf}(t) = \mathrm{e}^{-t^2}\left[1 + \frac{2\mathrm{i}}{\sqrt{\pi}} \int_0^t \mathrm{e}^{z^2}\, \mathrm{d}z\right]. \tag{5}$$

The magnetic field components follow from

$$B_y = -\beta_r E_x/c \quad \text{and} \quad B_x = \beta_r E_y/c. \tag{6}$$

The Lorentz force acting on a particle with charge q is finally

$$\vec{F} = q(\vec{E} + \vec{v} \times \vec{B}). \tag{7}$$

4 Round beams

With the simplifying assumption of round beams ($\sigma_x = \sigma_y = \sigma$), one can re-write (7) in cylindrical coordinates:

$$\vec{F} = q(E_r + \beta c B_\Phi) \times \vec{r}. \tag{8}$$

From (2) and with $r^2 = x^2 + y^2$ one can immediately write the fields from (8) as

$$E_r = -\frac{ne}{4\pi\epsilon_0} \cdot \frac{\delta}{\delta r} \int_0^\infty \frac{\exp(-\frac{r^2}{(2\sigma^2+q)})}{(2\sigma^2+q)} \mathrm{d}q \tag{9}$$

and

$$B_\Phi = -\frac{ne\beta c\mu_0}{4\pi} \cdot \frac{\delta}{\delta r} \int_0^\infty \frac{\exp(-\frac{r^2}{(2\sigma^2+q)})}{(2\sigma^2+q)} \mathrm{d}q. \tag{10}$$

We find from (9) and (10) that the force (8) has only a radial component. The expressions (9) and (10) can easily be evaluated when the derivative is done first and $1/(2\sigma^2 + q)$ is used as integration variable. We can now express the radial force in a closed form (using $\epsilon_0\mu_0 = c^{-2}$):

$$F_r(r) = -\frac{ne^2(1+\beta^2)}{2\pi\epsilon_0} \cdot \frac{1}{r} \cdot \left[1 - \exp\left(-\frac{r^2}{2\sigma^2}\right)\right] \tag{11}$$

and, for the Cartesian components in the two transverse planes, we get

$$F_x(r) = -\frac{ne^2(1+\beta^2)}{2\pi\epsilon_0} \cdot \frac{x}{r^2} \cdot \left[1 - \exp\left(-\frac{r^2}{2\sigma^2}\right)\right] \tag{12}$$

and

$$F_y(r) = -\frac{ne^2(1+\beta^2)}{2\pi\epsilon_0} \cdot \frac{y}{r^2} \cdot \left[1 - \exp\left(-\frac{r^2}{2\sigma^2}\right)\right]. \tag{13}$$

The forces (12) and (13) are computed when the charges of the test particle and the opposing beam have opposite signs. For equally charged beams the forces change sign. The shape of the force as a function of the amplitude is given in Fig. 1.

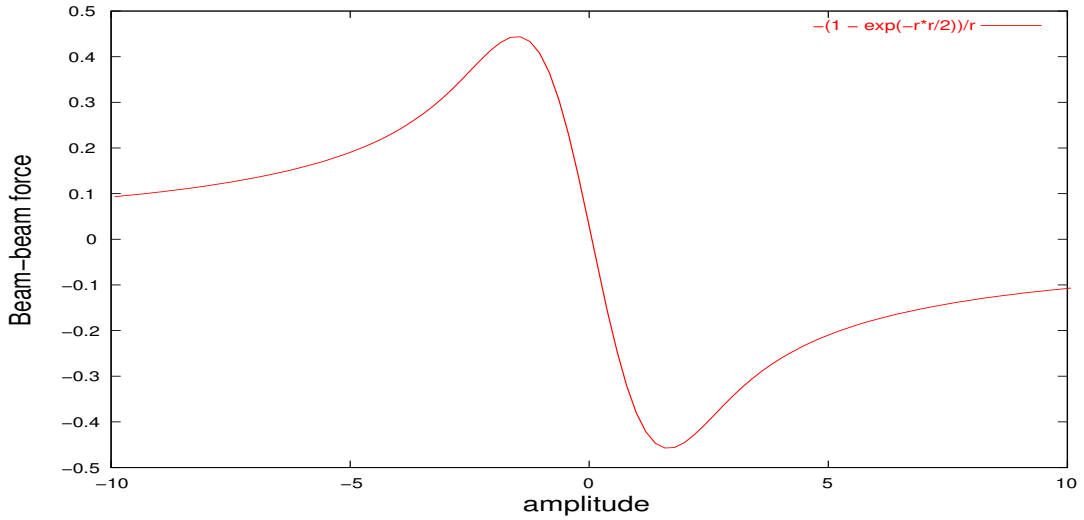

Fig. 1: Beam–beam force for round beams. Force in arbitrary units, amplitude in units of r.m.s. beam size

For small amplitudes the force is approximately linear and a particle crossing a beam at small amplitudes will experience a linear field. This results in a change of the tune as in a quadrupole. At larger amplitudes (i.e. above $\approx 1\sigma$) the force deviates strongly from this linear behaviour. Particles at larger amplitudes will also experience a tune change; however, this tune change will depend on the amplitude. From the analytical form (13) one can see that the beam–beam force includes higher multipoles.

5 Incoherent effects—single-particle effects

The force we have derived is the force of a beam on a single test particle. It can be used to study single-particle or incoherent effects. For that, we treat a particle crossing a beam as if it was moving through a static electromagnetic lens. We have to expect all effects that are known from resonance and non-linear theory, such as:

- unstable and/or irregular motion;
- beam blow up or bad lifetime.

6 Beam–beam parameter

We can derive the linear tune shift of a small-amplitude particle crossing a round beam of a finite length. We use the force to calculate the kick it receives from the opposing beam, i.e. the change of the slope of the particle trajectory. Starting from the two-dimensional force and multiplying with the longitudinal

distribution which depends on both position s and time t and which we assume has a Gaussian shape with a width of σ_s, we obtain

$$F_r(r,s,t) = -\frac{Ne^2(1+\beta^2)}{\sqrt{(2\pi)^3}\epsilon_0\sigma_s}\cdot\frac{1}{r}\cdot\left[1-\exp\left(-\frac{r^2}{2\sigma^2}\right)\right]\cdot\left[\exp\left(-\frac{(s+vt)^2}{2\sigma_s^2}\right)\right].$$

Here N is the total number of particles. We make use of Newton's law and integrate over the collision to get the radial deflection:

$$\Delta r' = \frac{1}{mc\beta\gamma}\int_{-\infty}^{\infty} F_r(r,s,t)\mathrm{d}t.$$

The radial kick $\Delta r'$ a particle with a radial distance r from the opposing beam centre receives is then

$$\Delta r' \;=\; -\frac{2Nr_0}{\gamma}\cdot\frac{1}{r}\cdot\left[1-\exp\left(-\frac{r^2}{2\sigma^2}\right)\right], \tag{14}$$

where we have re-written the constants and used the classical particle radius:

$$r_0 = e^2/4\pi\epsilon_0 mc^2, \tag{15}$$

where m is the mass of the particle. For small amplitudes r one can derive the asymptotic limit:

$$\Delta r'|_{r\to 0} \;=\; -\frac{Nr_0 r}{\gamma\sigma^2} \;=\; -\,r\,\cdot\,f. \tag{16}$$

This limit is the slope of the force at $r = 0$ and the force becomes linear with a focal length as the proportionality factor.

It is well known how the focal length relates to a tune change and one can derive a quantity ξ, which is known as the *linear beam–beam parameter*:

$$\xi \;=\; \frac{Nr_0\beta^*}{4\pi\gamma\sigma^2}. \tag{17}$$

Here r_0 is the classical particle radius (e.g. $r_\mathrm{e}, r_\mathrm{p}$) and β^* is the optical amplitude function (β-function) at the interaction point.

For small values of ξ and a tune far enough away from linear resonances this parameter is equal to the linear tune shift ΔQ.

The beam–beam parameter can be generalized for the case of non-round beams and becomes

$$\xi_{x,y} \;=\; \frac{Nr_0\beta^*_{x,y}}{2\pi\gamma\sigma_{x,y}(\sigma_x+\sigma_y)}. \tag{18}$$

The beam–beam parameter is often used to quantify the strength of the beam–beam interaction; however, it does not reflect the non-linear nature.

7 Non-linear effects

Since the beam–beam forces are strongly non-linear, the study of beam–beam effects encompasses the entire field of non-linear dynamics [8] as well as collective effects.

First we briefly discuss the immediate effect of the non-linearity of the beam–beam force on a single particle. It manifests as an amplitude-dependent tune shift and for a beam with many particles as a tune spread. The instantaneous tune shift of a particle when it crosses the other beam is related to the derivative of the force with respect to the amplitude $\delta F/\delta x$. For a particle performing an oscillation with

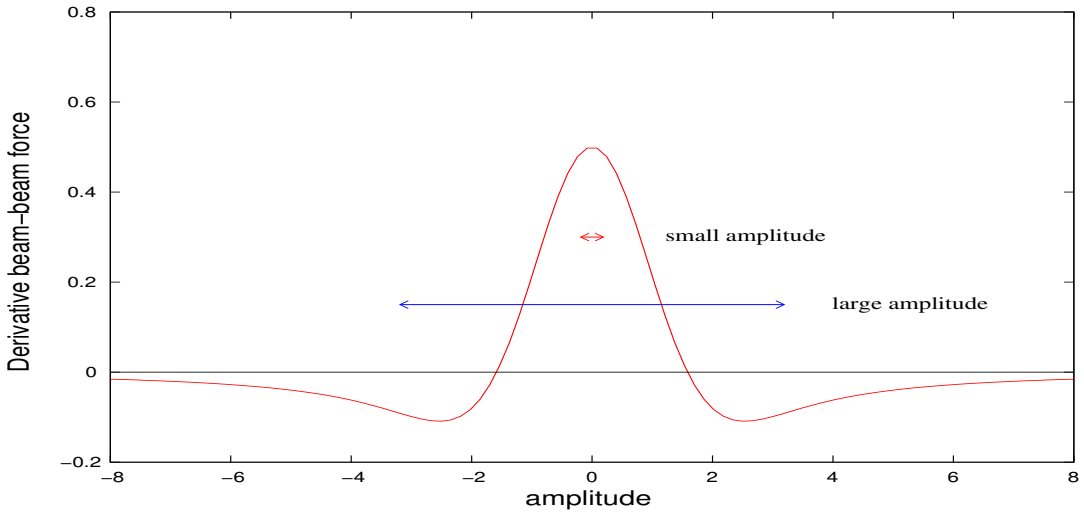

Fig. 2: Derivative of beam–beam force for round beams. Oscillation range of particles with large and small amplitudes.

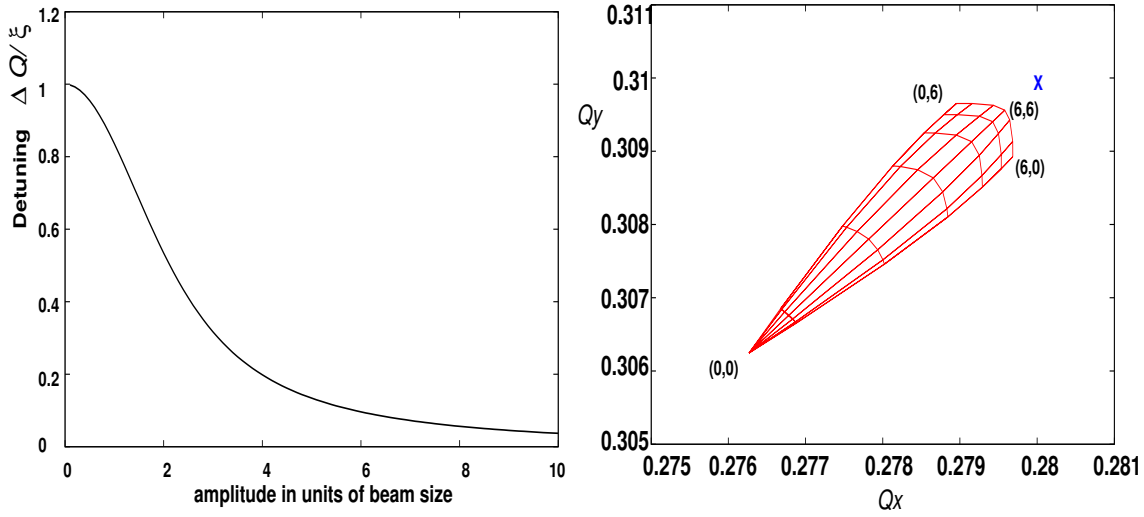

Fig. 3: Tune shift (non-linear detuning) as a function of the amplitude (left) and two-dimensional tune footprint (right).

a given amplitude the tune shift is calculated by averaging the slopes of the force over the range (i.e. the phases) of the particle's oscillation amplitudes.

The derivative of the beam–beam force from Fig. 1 is plotted for the one-dimensional case in Fig. 2.

The derivation of the detuning is given in Appendix B, using a classical method. An elegant calculation can be done using the Hamiltonian formalism [3] developed for non-linear dynamics and as discussed in [8] using the Lie formalism. It is demonstrated in Appendix C for one and two interaction points and includes the computation of the invariant Hamiltonian. We get the formula for the non-linear detuning with the amplitude J:

$$\Delta Q(J) \;=\; \xi \;\cdot\; \frac{2}{J} \;\cdot\; (1 - I_0(J/2) \cdot \mathrm{e}^{-J/2}), \tag{19}$$

where $I_0(x)$ is the modified Bessel function and $J = \epsilon\beta/2\sigma^2$ in the usual units. Here ϵ is the particle 'emittance' and not the beam emittance.

In the two-dimensional case, the tune shifts (ΔQ_x, ΔQ_y) of a particle with amplitudes x and y depend on both horizontal and vertical amplitudes. The detuning must be computed and presented in a two-dimensional form, i.e. the amplitude (x, y) is mapped into the tune space (Q_x, Q_y) or alternatively to the two-dimensional tune change (ΔQ_x, ΔQ_y). Such a presentation is usually called a 'tune footprint' and an example is shown in Fig. 3 (right); it maps the amplitudes into the tune space and each 'knot' of the mesh corresponds to a pair of amplitudes. Amplitudes between 0 and 6σ in both planes are used. The cross indicates the original, unperturbed tunes without the beam–beam interaction.

The maximum tune spread for a single head-on collision is equal to the tune shift of a particle with small amplitudes and for small tune shifts is equal to the beam–beam parameter ξ. In the simple case of a single head-on collision the parameter ξ is therefore a measure for the tune spread in the beam.

8 Beam stability

When the beam–beam interaction becomes too strong, the beam can become unstable or the beam dynamics is strongly distorted. One can distinguish different types of distortions, and a few examples are:

- non-linear motion can become stochastic and can result in a reduction of the dynamic aperture and particle loss and bad lifetime;
- distortion of beam optics: dynamic beta (LEP) [2];
- vertical blow up above the so-called beam–beam limit.

Since the beam–beam force is very non-linear, the motion can become 'chaotic'. This often leads to a reduction of the available dynamic aperture. The dynamic aperture is the maximum amplitude where the beam remains stable. Particles outside the dynamic aperture can eventually get lost. The dynamic aperture is usually evaluated by tracking particles with a computer program through the machine where they experience the fields from the machine elements and other effects such as wake fields or the beam–beam interaction.

Since the beam–beam interaction is basically a very non-linear lens in the machine, it distorts the optical properties and it may create a noticeable beating of the β-function around the whole machine and at the location of the beam–beam interaction itself. This can be approximated by inserting a quadrupole which produces the same tune shift at the position of the beam–beam interaction. The r.m.s. beam size at the collision point is now proportional to $\sqrt{\beta^*_{\rm p}}$, where $\beta^*_{\rm p}$ is the perturbed β-function, which can be significantly different from the unperturbed β-function β^*. This in turn changes the strength of the beam–beam interaction and the parameters have to be found in a self-consistent form. This is called the dynamic beta effect. This is a first deviation from our assumption that the beams are static non-linear lenses. A strong dynamic beta effect was found in LEP [11] due to its very large tune shift parameters.

Another effect that can be observed in particular in e^+e^- colliders is the blow up of the emittance, which naturally limits the reachable beam–beam tune shifts.

9 Beam–beam limit

In e^+e^- colliders the beam sizes are usually an equilibrium between the damping due to the synchrotron radiation and heating mechanisms such as quantum excitation, intra-beam scattering and, very importantly, the beam–beam effect. This leads to a behaviour that is not observed in a hadron collider. When the luminosity is plotted as a function of the beam intensity, it should increase approximately as the current squared [12], in agreement with

$$\mathcal{L} = \frac{N^2 \cdot kf}{4\pi\sigma_x\sigma_y}. \tag{20}$$

Here k is the number of bunches per beam and f the revolution frequency [12]. At the same time the beam–beam parameter ξ should increase linearly with the beam intensity according to (18):

$$\xi_y = \frac{N \cdot r_e \beta_y}{2\pi\gamma\sigma_y(\sigma_x + \sigma_y)}. \tag{21}$$

In all e^+e^- colliders the observation can be made that above a certain current, the luminosity increases approximately proportionally to the current, or at least much less than with the second power [10]. Another observation is that at the same value of the intensity the beam–beam parameter ξ saturates. This is shown for three e^+e^- colliders in Fig. 4 and schematically illustrated in Fig. 5. This limiting value of ξ is commonly known as the *beam–beam limit*.

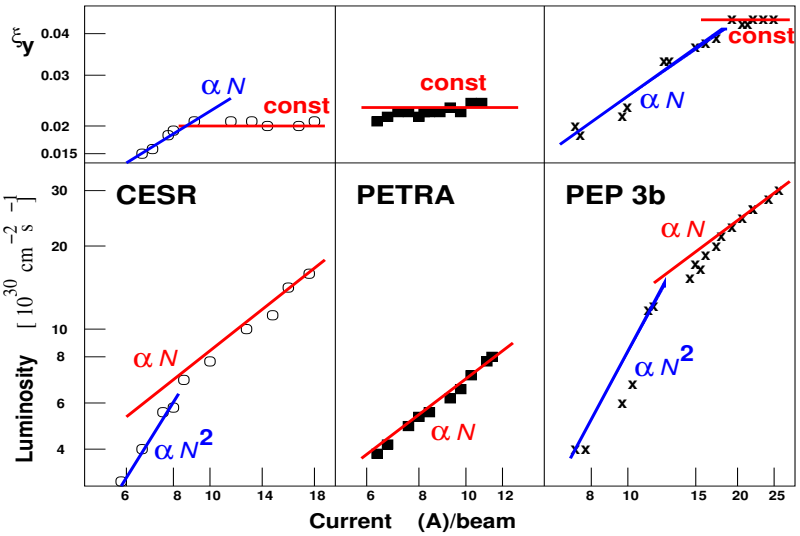

Fig. 4: Measurements of luminosity and beam–beam limit in e^+e^- colliders. Logarithmic scale of the axes to demonstrate change of exponent.

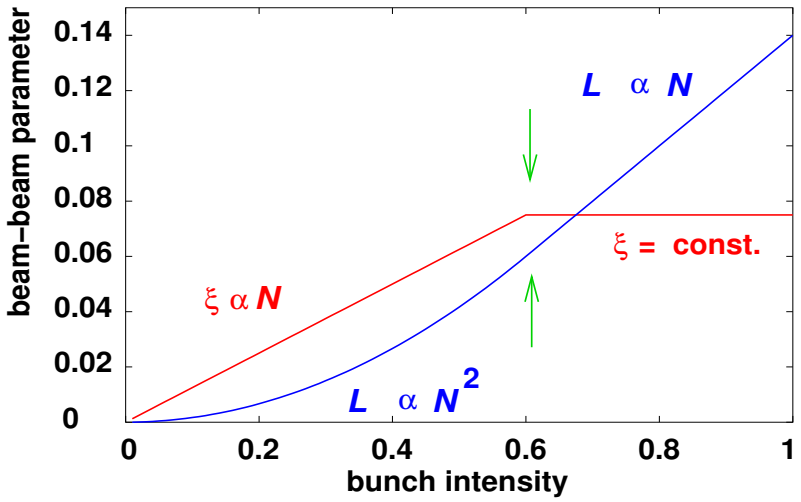

Fig. 5: Schematic illustration of beam–beam limit in e^+e^- colliders

When we re-write the luminosity as

$$\mathcal{L} = \frac{N^2 \cdot kf}{4\pi\sigma_x\sigma_y} = \frac{N \cdot kf}{4\pi\sigma_x} \cdot \frac{N}{\sigma_y}, \tag{22}$$

we get an idea of what is happening. In e^+e^- colliders the horizontal beam size σ_x is usually much larger than the vertical beam size σ_y and changes very little. In order for the luminosity to increase proportionally to the number of particles N, the factor N/σ_y must be constant.

This implies that with increasing current the vertical beam size increases in proportion above the beam–beam limit. This has been observed in all e^+e^- colliders and, since the vertical beam size is usually small, this emittance growth can be very substantial before the lifetime of the beam is affected or beam losses are observed.

The dynamics of machines with high synchrotron radiation is dominated by the damping properties and the beam–beam limit is not a universal constant nor can it be predicted. Simulation of beams with many particles can provide an idea of the order of magnitude [16, 17].

10 Crossing angle

To reach the highest luminosity, it is desirable to operate a collider with as many bunches as possible, since the luminosity is proportional to their number [12].

In a single-ring collider such as the SPS, Tevatron or LEP, the operation with k bunches leads to $2{\cdot}k$ collision points. When k is a large number, most of them are unwanted and must be avoided to reduce the perturbation due to the beam–beam effects.

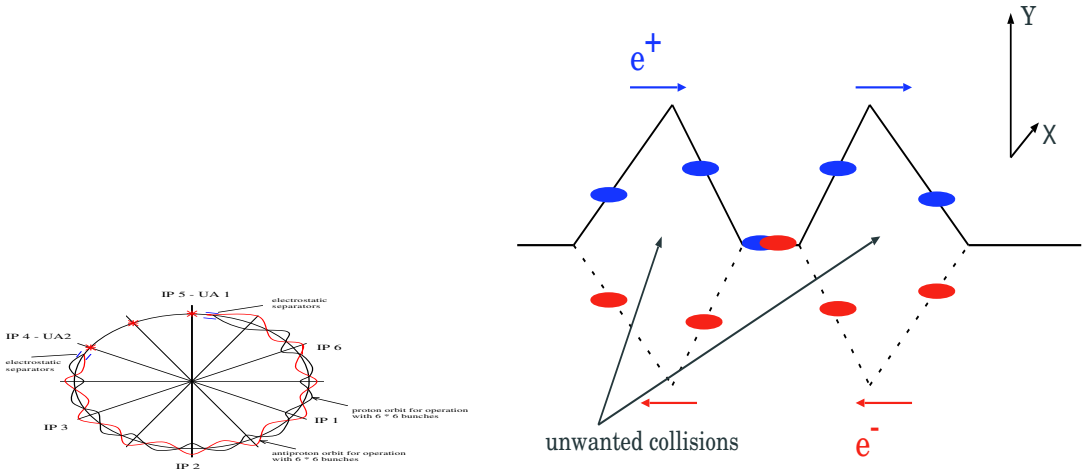

Fig. 6: Beam separation with a Pretzel scheme (SPS, Tevatron, LEP, left) and with short bunch trains (LEP, right)

Various schemes have been used to avoid these unwanted 'parasitic' interactions. Two prominent examples are shown in Fig. 6. In the SPS, Tevatron and LEP so-called Pretzel schemes were used. When the bunches are equidistant, this is the most promising method. When two beams of opposite charge travel in the same beam pipe, they can be moved onto separate orbits using electrostatic separators. In a well-defined configuration the two beams cross when the beams are separated (Fig. 6, left). To avoid a separation around the whole machine, the bunches can be arranged in so-called trains of bunches following each other closely. In that case a separation with electrostatic separators is only needed around the interaction regions. Such a scheme was used in LEP in the second phase [9] and it is schematically illustrated in Fig. 6 (right).

Contrary to the majority of the colliders, the LHC collides particles of the same type, which therefore must travel in separate beam pipes.

At the collision points of the LHC the two beams are brought together and into collision (Fig. 7). An arrangement of separation and recombination magnets is used for the purpose of making the beams cross (Fig. 8).

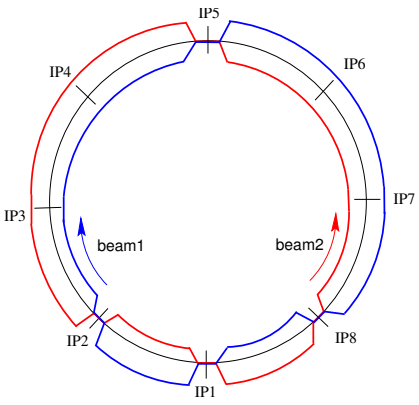

Fig. 7: Schematic layout of the LHC collision points and beams

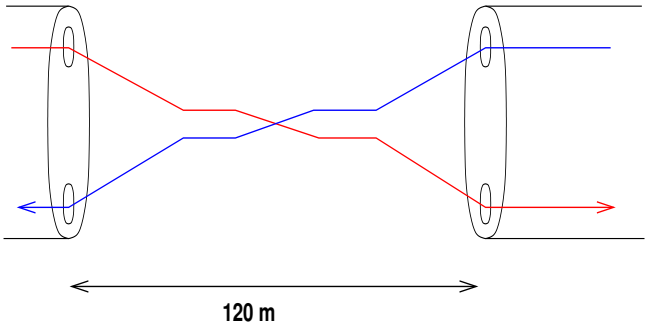

Fig. 8: Crossover between inner and outer vacuum chambers in the LHC (schematic)

During that process it is unavoidable that the beams travel in a common vacuum chamber for more than 120 m. In the LHC the time between the bunches is only 25 ns and therefore the bunches will meet in this region. In order to avoid the collisions, the bunches collide at a small crossing angle of 285 μrad.

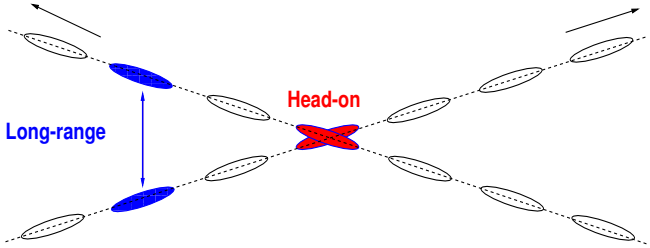

Fig. 9: Head-on and long-range interactions in a LHC interaction point

The basic principle is shown in Fig. 9: while two bunches collide at a small angle (quasi head on) at the centre, the other bunches are kept separated by the crossing angle. However, since they travel in a common beam pipe, the bunches still feel the electromagnetic forces from the bunches of the opposite beam. When the separation is large enough, these so-called long-range interactions should be weak. From the bunch spacing and the length of the interaction region one can easily calculate that at each of the four LHC interaction points we must expect 30 of these long-range encounters, i.e. in total 120 interactions. The typical separation between the two beams is between 7 and 10 in units of the beam size of the opposing beam.

10.1 Long-range beam–beam effects

Although the long-range interactions distort the beams much less than a head-on interaction, their large number and some particular properties require careful studies.

- They break the symmetry between planes, i.e. odd resonances are also excited.
- While the effect of head-on collisions is strongest for small-amplitude particles, they mostly affect particles at large amplitudes.
- The tune shift caused by long-range interactions has *opposite* sign in the plane of separation compared to the head-on tune shift.
- They cause changes of the closed orbit.
- They largely enhance the so-called PACMAN effects.

10.1.1 Opposite-sign tune shift

The opposite sign of the tune shift can easily be understood when we come back to the method for calculating the tune spread, explained with the help of Fig. 2.

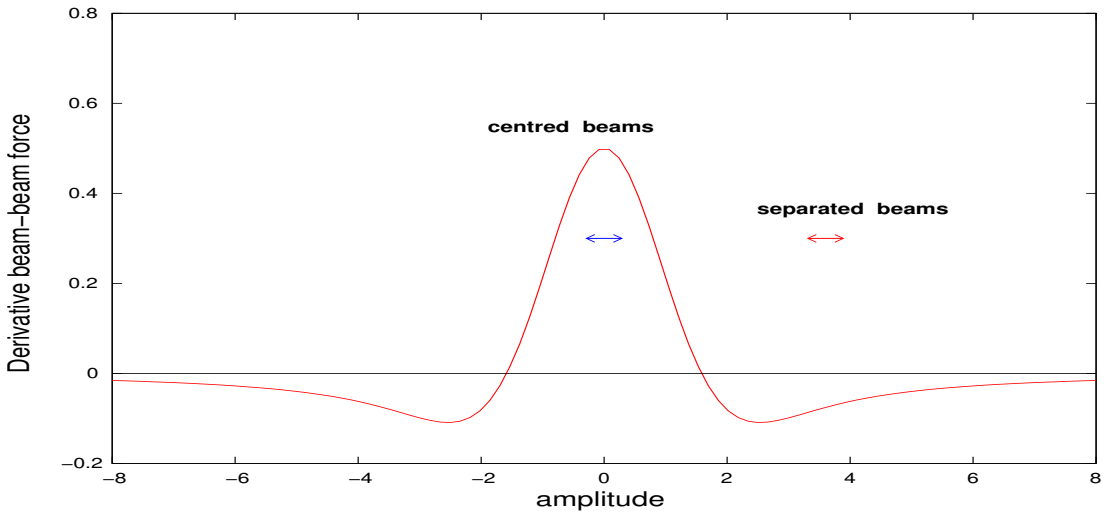

Fig. 10: Derivative of beam–beam force for round beams. Oscillation range of particles of centred and separated beams.

We average again the oscillation of a small-amplitude particle as it samples the focusing force of the beam–beam interaction. In Fig. 10, we show the range of oscillation for central collisions and for the interaction of separated beams, in both cases for particles with small oscillation amplitudes. When the separation is larger than $\approx 1.5\sigma$, the focusing (slope of the force as a function of the amplitude) changes sign and the resulting tune shift assumes the opposite sign.

To some extent, this property could be used to partially compensate long-range interactions when a configuration is used where the beams are separated in the horizontal plane in one interaction region and in the vertical plane in another one.

10.1.2 Strength of long-range interactions

The geometry of a single encounter is shown in Fig. 11. The particles in the test bunch receive a kick (change of slope) $\Delta x'$.

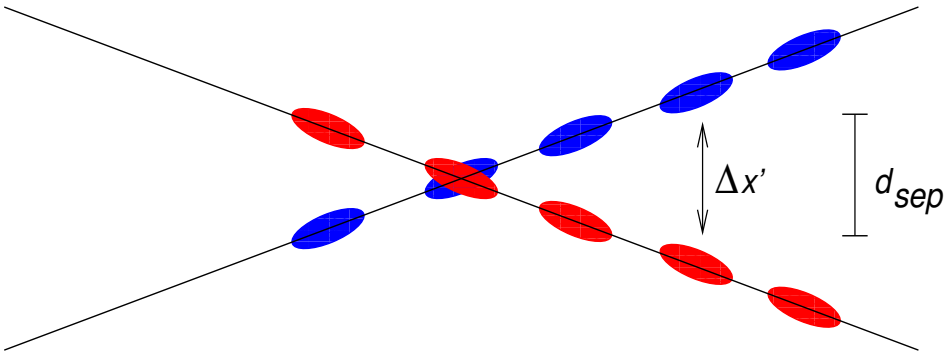

Fig. 11: Long-range interaction, schematic

Assuming a separation d in the horizontal plane, the kicks in the two planes can be written as

$$\Delta x' = -\frac{2Nr_0}{\gamma} \cdot \frac{(x+d)}{r^2} \cdot \left[1 - \exp\left(-\frac{r^2}{2\sigma^2}\right)\right] \tag{23}$$

with $r^2 = (x+d)^2 + y^2$. The equivalent formula for the plane orthogonal to the separation is

$$\Delta y' = -\frac{2Nr_0}{\gamma} \cdot \frac{y}{r^2} \cdot \left[1 - \exp\left(-\frac{r^2}{2\sigma^2}\right)\right]. \tag{24}$$

It is fairly obvious that the effect of long-range interactions must strongly depend on the separation. The calculation shows that the tune spread ΔQ_{lr} from long-range interactions alone follows an approximate scaling (for large enough separation, i.e. above $\approx 6\sigma$):

$$\Delta Q_{\mathrm{lr}} \propto -\frac{N}{d^2}, \tag{25}$$

where N is the bunch intensity and d the separation. Small changes in the separation can therefore result in significant differences.

10.1.3 Footprint for long-range interactions

Contrary to the head-on interaction where the small-amplitude particles are mostly affected, now the large-amplitude particles experience the strongest long-range beam–beam perturbations. This is rather intuitive, since the large-amplitude particles are the ones which can come closest to the opposing beam as they perform their oscillations. We must therefore expect a totally different tune footprint.

Such a footprint for only long-range interactions is shown in Fig. 12. Since the symmetry between the two planes is broken, the resulting footprint shows no symmetry. In fact, the tune shifts have different signs for x and y, as expected. For large amplitude one observes a 'folding' of the footprint. This occurs when large-amplitude particles are considered, for which the oscillation amplitudes extend across the central maximum in Fig. 10, i.e. when the oscillation amplitude is larger than the separation between the beams.

Such large amplitudes are treated in Fig. 10 to demonstrate this feature. In practice, these amplitudes are usually not important since in real machines no particles reach these amplitudes.

In Fig. 13 (left), we show separately the footprints for two head-on proton–proton collisions, and long-range interactions with horizontal separation and vertical separation, respectively.

The differences and in particular the different sign of the long-range tune shift are clearly visible. The long-range footprints are shifted away from the original tune (0.28, 0.31) in opposite directions. Amplitudes between 0 and 6σ are shown in the figure. In the same figure on the right we show the

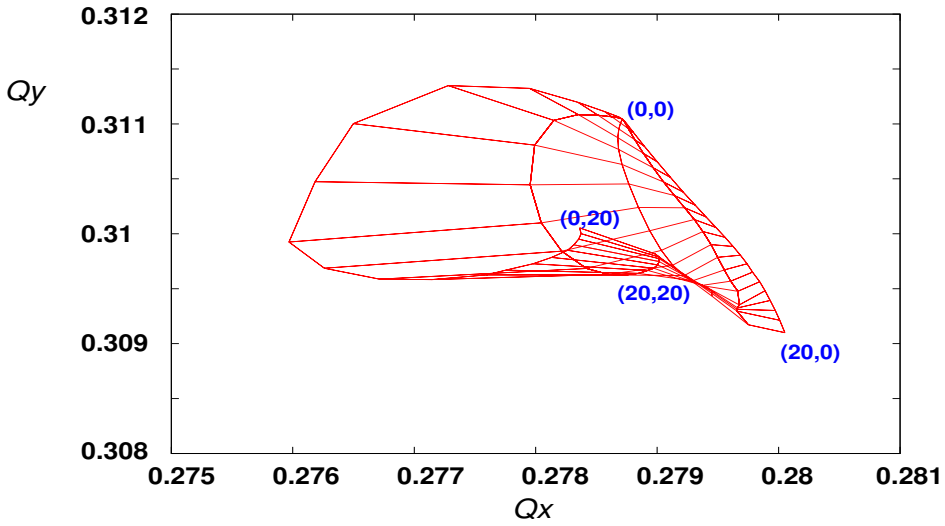

Fig. 12: Tune footprint for long-range interactions only. Vertical separation and amplitudes between 0 and 20σ

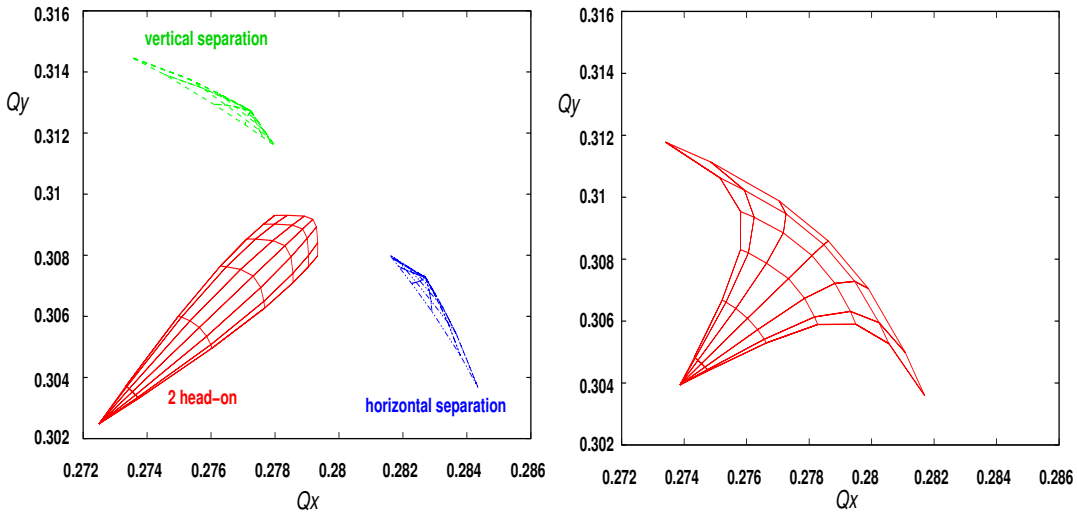

Fig. 13: Footprint for two head-on interactions (proton–proton), long-range interactions in the horizontal plane and long-range interactions in the vertical plane (left). Combined head-on and long-range interactions, one horizontal and one vertical crossing (right).

combined footprint, i.e. for particles which experience two head-on collisions, long-range interactions in one interaction point with horizontal separation and a second with vertical separation. A partial compensation can be seen and the footprint is again symmetric in x and y. In particular, the linear tune shifts of the central parts are very well compensated.

10.1.4 Dynamic aperture reduction due to long-range interactions

For too small separation, the tune spread induced by long-range interactions can become very large and resonances cannot be avoided any more. The motion can become irregular and as a result particles at large amplitudes can get lost.

This is demonstrated in Fig. 14. The emittance increase of a large-amplitude particle (5σ) is computed for different values of the crossing angle and hence of the beam separation. For large enough

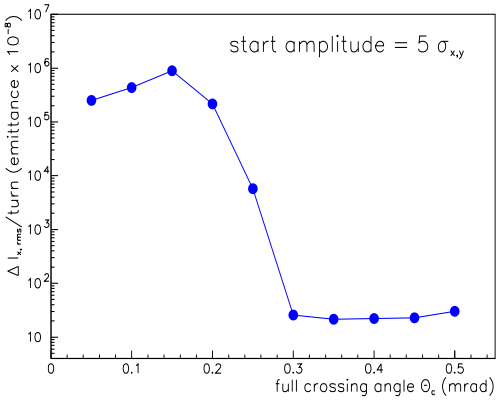

Fig. 14: Emittance increase as function of crossing angle

angles the emittance increase is very small, but it increases over several orders of magnitude when the crossing angle drops significantly below 300 μrad. These results are obtained by particle tracking [13, 14].

To evaluate the dynamic aperture in the presence of beam–beam interactions, a simulation of the complete machine is necessary and the interplay between the beam–beam perturbation and possible machine imperfections is important [15].

For the present LHC parameters we consider the minimum crossing angle to be 285 μrad.

11 Beam–beam-induced orbit effects

When two beams do not collide exactly head on, the force has a constant contribution, which can easily be seen when the kick $\Delta x'$ (from (23), for sufficiently large separation) is developed in a series:

$$\Delta x' \;=\; \frac{\text{const.}}{d} \cdot \left[\; 1 \;-\; \frac{x}{d} \;+\; O\left(\frac{x^2}{d^2}\right) \;+\; \cdots \right]. \tag{26}$$

A constant contribution, i.e. more precisely an amplitude-independent contribution, changes the orbit of the bunch as a whole (Fig. 15).

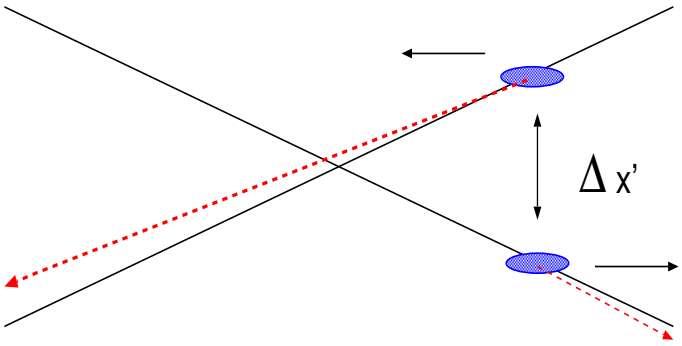

Fig. 15: Beam–beam deflection leading to orbit changes

When the beam–beam effect is strong enough, i.e. for high intensity and/or small separation, the orbit effects are large enough to be observed.

When the orbit of a beam changes, the separation between the beams will change as well, which in turn will lead to a slightly different beam–beam effect and so on. The orbit effects must therefore be computed in a self-consistent way [18], in particular when the effects are sizable. The closed orbit of

an accelerator can usually be corrected; however, an additional effect, which is present in some form in many colliders, sets a limit to the correction possibilities. A particularly important example is the LHC and we shall therefore use it to illustrate this feature.

12 PACMAN bunches

The bunches in the LHC do not form a continuous train of equidistant bunches spaced by 25 ns, but some empty space must be provided to allow for the rise time of kickers. These gaps and the number of bunches per batch are determined by requirements from the LHC injectors (PS, SPS etc) and the preparation of the LHC beam (bunch splitting). The whole LHC bunch pattern is composed of 39 smaller batches (trains of 72 bunches) separated by gaps of various length followed by a large abort gap for the dump kicker at the end. Figure 16 shows the actual LHC filling scheme with the various gaps in the train.

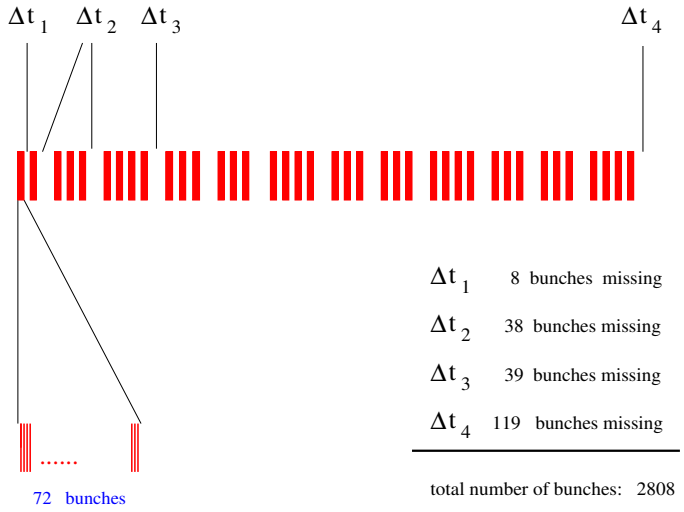

Fig. 16: Bunch filling scheme in the LHC

In the LHC, only 2808 out of 3564 possible bunches are present with the above filling scheme. Due to the symmetry, bunches normally meet other bunches at the head-on collision point. For the long-range interactions this is no longer the case.

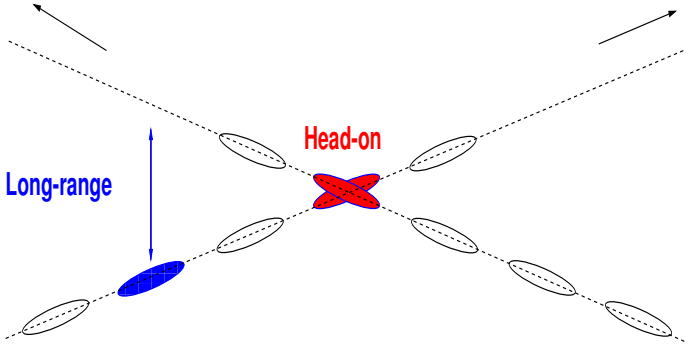

Fig. 17: Long-range interactions with missing bunches

This is illustrated in Fig. 17. Bunches at the beginning and at the end of a small batch will encounter a hole and as a result experience fewer long-range interactions than bunches from the middle of a batch [19]. In the limit, the first bunch of a batch near a large gap encounters no opposing bunch before the central collision and the full number of bunches after.

Bunches with fewer long-range interactions have a very different integrated beam–beam effect and a different dynamics must be expected. In particular, they will have a different tune and occupy a different area in the working diagram; therefore, they may be susceptible to resonances which can be avoided for nominal bunches. The overall space needed in the working diagram is therefore largely increased [19, 20].

Another consequence of reduced long-range interactions is the different effect on the closed orbit of the bunches. We have to expect a slightly different orbit from bunch to bunch.

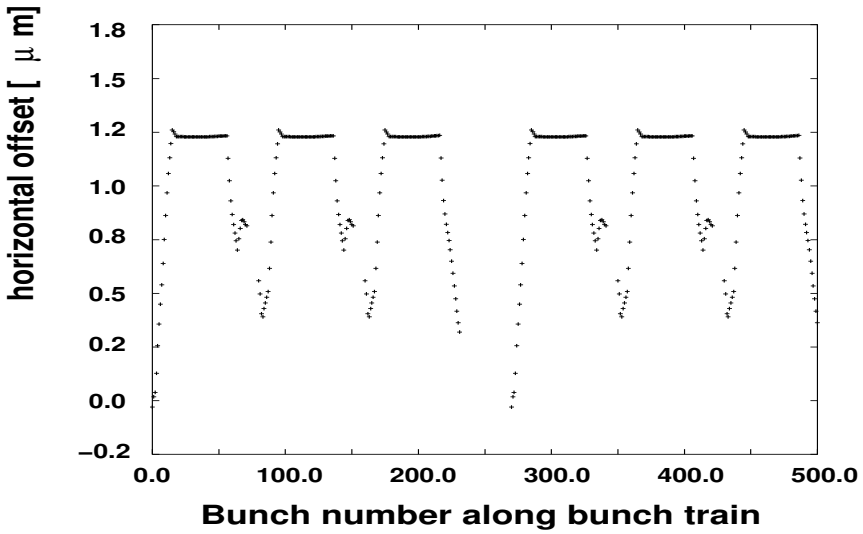

Fig. 18: Horizontal orbits of the first 432 bunches at IP1

This effect is demonstrated in Fig. 18, where we show the horizontal position at one head-on collision point for 432 bunches (out of 2808). The bunches in the middle of a batch have all interactions and therefore the same orbit while the bunches at the beginning and end of a batch show a structure which exhibits the decreasing number of long-range interactions. The orbit spread is approximately 10–15% of the beam size. Since the orbits of the two beams are not the same, it is impossible to make all bunches collide exactly head on. A significant fraction will collide with an offset. Although the immediate effect on the luminosity is small [12], collisions at an offset can potentially affect the dynamics and are undesirable. The LHC design should try to minimize these offsets [19, 20].

A second effect, the different tunes of the bunches, is shown in Fig. 19. For three batches it shows a sizable spread from bunch to bunch and without compensation effects [20] it may be too large for a safe operation.

13 Coherent beam–beam effects

So far we have mainly studied how the beam–beam interaction affects the single-particle behaviour and treated the beam–beam interaction as a static lens. In the literature this is often called a ‘weak–strong’ model: a ‘weak’ beam (a single particle) is perturbed by a ‘strong’ beam (not affected by the weak beam). When the beam–beam perturbation is important, the model of an unperturbed, strong beam is not valid any more, since its parameters change under the influence of the other beam and vice versa. When this is the case, we talk about so-called ‘strong–strong’ conditions. The first example of such a ‘strong–strong’ situation was the orbit effect where the beams mutually changed their closed orbits. These closed orbits had to be found in a self-consistent way. This represents a static strong–strong effect.

In the next step we investigate dynamic effects under the strong–strong condition [29]. When we consider the coherent motion of bunches, the collective behaviour of all particles in a bunch is studied. A coherent motion requires an organized behaviour of all particles in a bunch. A typical example are

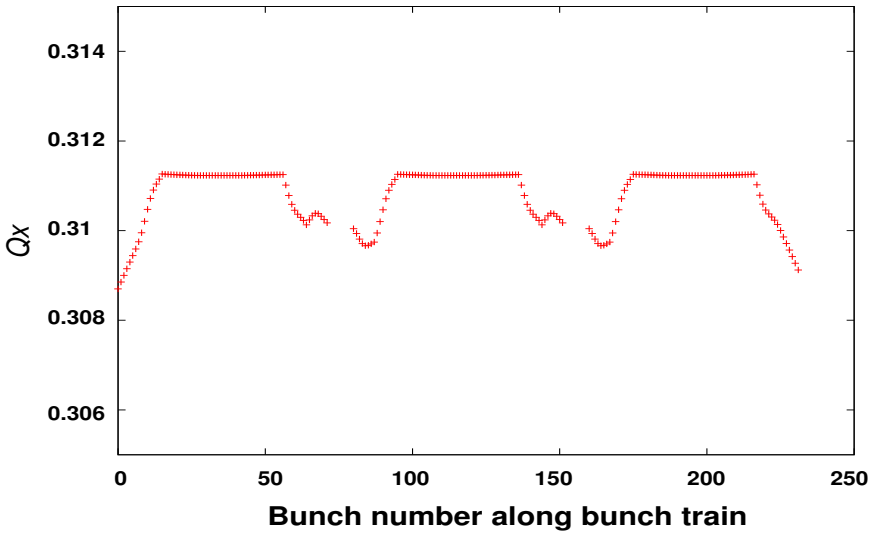

Fig. 19: Tune variation along the LHC bunch pattern

oscillations of the centre of mass of the bunches, so-called dipole oscillations. Such oscillations can be driven by external forces such as impedances and may be unstable. At the collision of two counter-rotating bunches not only the individual particles receive a kick from the opposing beam, but the bunch as an entity gets a coherent kick. This coherent kick of separated beams can excite coherent dipole oscillations. Its strength depends on the distance between the bunch centres at the collision point. It can be computed by adding the individual contributions of all particles. For small distances it can be shown [1, 24] that it is just one-half of the incoherent kick a single particle would receive at the same distance. For distances large enough, the incoherent and coherent kicks become the same.

14 Coherent beam–beam modes

To understand the dynamics of dipole oscillations, we first study the simplest case with one bunch in each beam.

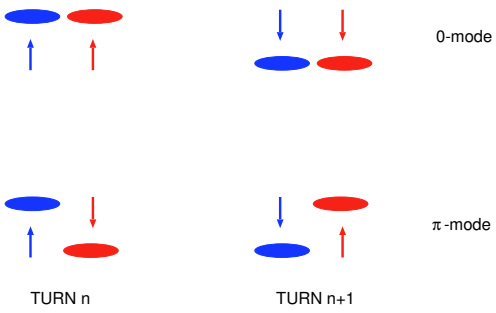

Fig. 20: Basic dipole modes of two bunches. Relative position of the bunches at the interaction point at two consecutive turns.

When the bunches meet turn after turn at the collision point, their oscillation can either be exactly in phase (0 degree phase difference) or out of phase (180 degrees or π phase difference). Any other oscillation can be constructed from these basic modes. The modes are sketched very schematically in Fig. 20. The relative positions of the bunches as observed at the interaction point are shown for two consecutive turns n and $n+1$. The first mode is called the 0-mode (or sometimes called the σ-mode) and the second the π-mode. In the first mode the distance between the bunches does not change turn by turn

and therefore there is no net force driving an oscillation. This mode must oscillate with the unperturbed frequency (tune) Q_0. For the second mode the net force difference between two turns is a maximum and the tune becomes $Q_0 + \Delta Q_{\rm coh}$. The sign of $\Delta Q_{\rm coh}$ depends whether the two beams have equal charge (defocusing case) or opposite charge (focusing case). The calculation of $\Delta Q_{\rm coh}$ is non-trivial: when the bunches are considered as rigid objects, the tune shift can be computed easily using the coherent kick but is underestimated [21]. The correct calculation must allow for changes of the density distribution during the collision and, moreover, must allow a deviation from a Gaussian function. The computation requires us to solve the Vlasov equation of two coupled beams [25–28].

The 0-mode is found at the unperturbed tune, as expected. The π-mode is shifted by 1.2–1.3ξ. The precise value depends on the ratio of the horizontal and vertical beam sizes [26]. We have seen before the incoherent tune spread (footprint) the individual particles occupy and we know that it spans the interval [0.0, 1.0] ξ, starting at the 0-mode.

Here one can make an important observation: under the strong–strong condition the π-mode is a discrete mode outside the incoherent spectrum [27, 28]. This has dramatic consequences for the stability of the beams. A coherent mode that is outside an incoherent frequency spectrum cannot be stabilized by Landau damping. Under these conditions the coherent beam–beam effect could drive the dipole oscillation to large amplitudes and may result in the loss of the beam. Observations of the coherent beam–beam effects have been made at PETRA [21]. Beam–beam modes have been observed with high-intensity coasting beams in the ISR [22] and recently in a bunched hadron collider at RHIC [23].

Coherent beam–beam modes can be driven by head-on collisions with a small offset or by long-range interactions. In the first case and for small oscillations, the problem can be linearized and the theoretical treatment is simplified. The forces from long-range interactions are very non-linear but the numerical evaluation is feasible. Since the coherent shift must have the opposite sign for long-range interactions, the situation is very different. In particular, the π-mode from long-range interactions alone would appear on the opposite side of the 0-mode in the frequency spectrum [28, 30]. Both the incoherent and the coherent spectra include both types of interactions.

15 Compensation of beam–beam effects

For the case where the beam–beam effects limit the performance of a collider, several schemes have be proposed to compensate all or part of the detrimental effects. The basic principle is to design correction devices which act as non-linear 'lenses' to counteract the distortions from the non-linear beam–beam 'lens'.

For both head-on and long-range effects schemes have been proposed:

- head-on effects:
  - electron lenses;
  - linear lens to shift tunes;
  - non-linear lens to decrease tune spread;
- long-range effects:
  - at large distance: beam–beam force changes like $1/r$;
  - same force as a wire.

16 Electron lenses

The basic principle of a compensation of proton–proton (or –antiproton) collisions with an 'electron lens' implies that the proton (antiproton) beam travels through a counter-rotating high-current electron beam ('electron lens') [31, 32]. The negative electron space charge can reduce the effect from the collision with the other proton beam.

An electron beam with a size much larger than the proton beam can be used to shift the tune of the proton beam ('linear lens'). When the current in the electron bunches can be varied fast enough, the tune shift can be different for the different proton bunches, thus correcting PACMAN tune shifts.

When the electron charge distribution is chosen to be the same as the counter-rotating proton beam, the non-linear focusing of this proton beam can be compensated ('non-linear lens'). When it is correctly applied, the tune spread in the beam can be strongly reduced.

Such lenses have been constructed at the Tevatron at Fermilab [32] and experiments are in progress.

17 Electrostatic wire

To compensate the tune spread from long-range interactions, one needs a non-linear lens that resembles a separated beam. At large enough separation, the long-range force changes approximately with $\frac{1}{r}$ and this can be simulated by a wire parallel to the beam [33].

In order to compensate PACMAN effects, the wires have to be pulsed according to the bunch filling scheme. Tests are in progress at the SPS to study the feasibility of such a compensation for the LHC.

18 Möbius scheme

The beam profiles of e^+e^- colliders are usually flat, i.e. the vertical beam size is much smaller than the horizontal beam size. Some studies indicate that the collision of round beams, even for e^+e^- colliders, shows more promise for higher luminosity since larger beam–beam parameters can be achieved. Round beams can always be produced by strong coupling between horizontal and vertical planes. A more elegant way is the so-called Möbius lattice [34, 35]. In this lattice, the horizontal and vertical betatron oscillations are exchanged by an insertion. A horizontal oscillation in one turn becomes a vertical oscillation in the next turn and vice versa. Tests with such a scheme have been done at CESR at Cornell [35].

References

[1] W. Herr, Beam–beam effects, Proc. CERN Accelerator School, Zeuthen, 2003, CERN-2006-002 (2006), p. 379.

[2] A. Chao, The beam–beam instability, SLAC-PUB-3179 (1983).

[3] L. Evans and J. Gareyte, Beam–beam effects, CERN Accelerator School, Oxford, 1985, CERN 87-03 (1987), p. 159.

[4] A. Zholents, Beam–beam effects in electron–positron storage rings, Joint US–CERN School on Particle Accelerators (Lecture Notes in Physics No. 400, Springer, Heidelberg, 1992), p. 321.

[5] E. Keil, Beam–beam dynamics, CERN Accelerator School, Rhodes, 1993, CERN 95-06 (1995), p. 539.

[6] S. Kheifets, PETRA-Kurzmitteilung 119, DESY (1976).

[7] M. Basetti and G.A. Erskine, Closed expression for the electrical field of a two-dimensional Gaussian charge, CERN-ISR-TH/80-06 (1980).

[8] W. Herr, Mathematical and numerical methods for non-linear beam dynamics, these proceedings, CERN Accelerator School (2013).

[9] B. Goddard, W. Herr, E. Keil, M. Lamont, M. Meddahi and E. Peschardt, *Part. Accel.* **57** (1998) 237.

[10] J.T. Seeman, Observations of the beam–beam interaction (Lecture Notes in Physics No. 247, Springer, Heidelberg, 1986), p. 121.

[11] D. Brandt *et al.*, Is LEP beam–beam limited at its highest energy?, Proc. Particle Accelerator Conf., New York, 1999, p. 3005.

[12] W. Herr, Concept of luminosity, Proc. CERN Accelerator School, Zeuthen, 2003, CERN-2006-002 (2006), p. 361.

[13] T. Sen *et al.*, Effect of the beam–beam interactions on the dynamic aperture and amplitude growth in the LHC, Proc. Workshop on Beam–Beam Effects in Large Hadron Colliders, LHC99, Geneva, 12–17 April 1999, CERN-SL-99-039 (AP) (1999), p. 85.

[14] Y. Papaphilippou and F. Zimmermann, Weak–strong beam–beam simulations for the LHC, Proc. Workshop on Beam–Beam Effects in Large Hadron Colliders, LHC99, Geneva, 12–17 April 1999, CERN-SL-99-039 (AP) (1999), p. 95.

[15] Y. Luo and F. Schmidt, Dynamic aperture studies for LHC optics version 6.2 at collision, CERN LHC Project Note 310 (2003).

[16] S. Myers, *IEEE Trans. Nucl. Sci.* **NS-28** (1981) 2503.

[17] S. Myers, Review of beam–beam simulations (Lecture Notes in Physics No. 247, Springer, Heidelberg, 1986), p. 176.

[18] H. Grote and W. Herr, Self-consistent orbits with beam–beam effects in the LHC, Proc. 2001 Workshop on Beam–Beam Effects, Fermilab, Chicago, IL, 25–27 June 2001.

[19] W. Herr, Effects of PACMAN bunches in the LHC, CERN LHC Project Report 39 (1996).

[20] W. Herr, Features and implications of different LHC crossing schemes, LHC Project Report 628 (2003).

[21] A. Piwinski, *IEEE Trans. Nucl. Sci.* **NS-26** (1979) 4268.

[22] J.P. Koutchouk, ISR Performance Report – A numerical estimate of the coherent beam–beam effect in the ISR, CERN ISR-OP/JPK-bm (1982).

[23] W. Fischer *et al.*, Observation of coherent beam–beam modes in RHIC, BNL C-AD/AP/75 (2002).

[24] K. Hirata, *Nucl. Instrum. Methods* **A 269** (1988) 7.

[25] R.E. Meller and R.H. Siemann, *IEEE Trans. Nucl. Sci.* **NS-28** (1981) 2431.

[26] K. Yokoya *et al.*, *Part. Accel.* **27** (1990) 181.

[27] Y. Alexahin, *Part. Accel.* **59** (1996) 43.

[28] Y. Alexahin, *Nucl. Instrum. Methods* **A 380** (2002) 253.

[29] Y. Alexahin, H. Grote, W. Herr and M.P. Zorzano, Coherent beam–beam effects in the LHC, Presented at HEACC 2001, Tsukuba, Japan, CERN LHC Project Report 466 (2001).

[30] W. Herr, M.P. Zorzano and F. Jones, *Phys. Rev. ST Accel. Beams* **4** (2001) 054402.

[31] V.D. Shiltsev *et al.*, Compensation of beam–beam effects in the Tevatron collider with electron beams, Proc. Particle Accelerator Conf., New York, 1999, p. 3728.

[32] V.D. Shiltsev *et al.*, *Phys. Rev. ST Accel. Beams* **2** (1999) 071001.

[33] J.P. Koutchouk *et al.*, Correction of the long-range beam–beam effect in LHC using electromagnetic lenses, Proc. Particle Accelerator Conf., New York, 1999, p. 1681.

[34] R. Talman, *Phys. Rev. Lett.* **74** (1995) 1590.

[35] S. Henderson *et al.*, Investigation of the Möbius accelerator at CESR, CBN 99-5 (1999).

[36] L. Evans, The beam–beam interaction, CERN Accelerator Physics Course on Proton–Antiproton Colliders, CERN 84-15 (1984), p.319.

[37] O.D. Kellog, *Foundations of Potential Theory* (Dover, New York, 1953).

[38] A. Chao, P. Bambade and W. Weng, Non-linear beam–beam resonances (Lecture Notes in Physics No. 247, Springer, Heidelberg, 1986), p. 77.

[39] O. Brüning, Non-linear imperfections, these proceedings, CERN Accelerator School (2013).

[40] A.G. Webster, *Partial Differential Equations of Mathematical Physics* (Hafner, New York, 1950).

[41] I. Bronstein *et al.*, *Taschenbuch der Mathematik* (Harri Deutsch, Frankfurt, 2000).

[42] A. Dragt, *IEEE Trans. Nucl. Sci.* **NS-26** (1979) 3601.

[43] A. Dragt, Analysis of the beam–beam interaction using transfer maps, Proc. Beam–Beam Interaction Seminar, SLAC 1980, SLAC-PUB-2624 (1980).

[44] E. Forest, *Beam Dynamics, A New Attitude and Framework* (Harwood Academic, Berkeley, CA, 1998).

[45] A. Chao, Lecture notes on topics in accelerator physics, SLAC (2001).

[46] D. Kaltchev, On beam–beam resonances observed in LHC tracking, TRI-DN-07-9 (TRIUMF, Vancouver, Canada, 2007).

[47] W. Herr and D. Kaltchev, Effect of phase advance between interaction points in the LHC on the beam–beam interaction, CERN LHC Project 1082 (2008).

Appendices

A Appendix A

In practice, one usually derives the potential $U(x, y, z)$ from the Poisson equation, which relates the potential to the charge-density distribution $\rho(x, y, z)$:

$$\Delta U = -\frac{1}{\epsilon_0}\rho(x, y, z) \tag{A.1}$$

and computes the fields from

$$\vec{E} \;=\; -\nabla U(x, y, \sigma_x, \sigma_y). \tag{A.2}$$

The Poisson equation can be solved using e.g. the Green's function method (e.g. [40]) since the Green's function for this boundary value problem is well known. The formal solution using a Green's function $G(x, y, z, x_0, y_0, z_0)$ is

$$U(x, y, z) = \frac{1}{\epsilon_0}\int G(x, y, z, x_0, y_0, z_0)\cdot\rho(x_0, y_0, z_0)\mathrm{d}x_0\mathrm{d}y_0\mathrm{d}z_0. \tag{A.3}$$

For the solution of the Poisson equation, we get [41]

$$U(x, y, z, \sigma_x, \sigma_y, \sigma_z) = \frac{1}{4\pi\epsilon_0}\int\int\int \frac{\rho(x_0, y_0, z_0)\mathrm{d}x_0\mathrm{d}y_0\mathrm{d}z_0}{\sqrt{(x-x_0)^2+(y-y_0)^2+(z-z_0)^2}}. \tag{A.4}$$

In the case of a beam with Gaussian beam density distributions, we can factorize the density distribution $\rho(x_0, y_0, z_0) \;=\; \rho(x_0)\;\cdot\;\rho(y_0)\;\cdot\;\rho(z_0)$ with r.m.s. of σ_x, σ_y and σ_z:

$$\rho(x_0, y_0, z_0) = \frac{Ne}{\sigma_x\sigma_y\sigma_z(\sqrt{2\pi})^3}\mathrm{e}^{\left(-\frac{x_0^2}{2\sigma_x^2}-\frac{y_0^2}{2\sigma_y^2}-\frac{z_0^2}{2\sigma_z^2}\right)}. \tag{A.5}$$

Here N is the number of particles in the bunch. We therefore have

$$U(x, y, z, \sigma_x, \sigma_y, \sigma_z) = \frac{1}{4\pi\epsilon_0}\frac{Ne}{\sigma_x\sigma_y\sigma_z(\sqrt{2\pi})^3}\int\int\int \frac{\mathrm{e}^{\left(-\frac{x_0^2}{2\sigma_x^2}-\frac{y_0^2}{2\sigma_y^2}-\frac{z_0^2}{2\sigma_z^2}\right)}\mathrm{d}x_0\mathrm{d}y_0\mathrm{d}z_0}{\sqrt{(x-x_0)^2+(y-y_0)^2+(z-z_0)^2}}. \tag{A.6}$$

This is difficult to solve and we rather follow the proposal by Kheifets [6] and solve the diffusion equation

$$\Delta V - A^2 \cdot \frac{\delta V}{\delta t} = -\frac{1}{\epsilon_0}\rho(x,y,z) \qquad (\text{for } t \geq 0) \tag{A.7}$$

and obtain the potential U by going to the limit $A \rightarrow 0$, i.e.

$$U = \lim_{A \to 0} V. \tag{A.8}$$

The reason for this manipulation is that the Green's function to solve the diffusion equation takes a more appropriate form [41]:

$$G(x,y,z,t,x_0,y_0,z_0) = \frac{A^3}{(2\sqrt{\pi t})^3} \cdot \mathrm{e}^{-A^2/4t\cdot((x-x_0)^2+(y-y_0)^2+(z-z_0)^2)} \tag{A.9}$$

and we get for $V(x,y,z,\sigma_x,\sigma_y,\sigma_z)$:

$$\frac{Ne}{\sigma_x\sigma_y\sigma_z(\sqrt{2\pi})^3\epsilon_0}\int_0^t \mathrm{d}\tau \int\int\int \mathrm{e}^{\left(-\frac{x_0^2}{2\sigma_x^2}-\frac{y_0^2}{2\sigma_y^2}-\frac{z_0^2}{2\sigma_z^2}\right)} \frac{A^3 \cdot \mathrm{e}^{-A^2/4\tau((x-x_0)^2+(y-y_0)^2+(z-z_0)^2)}}{(2\sqrt{\pi\tau})^3} \mathrm{d}x_0\mathrm{d}y_0\mathrm{d}z_0. \tag{A.10}$$

This allows us to avoid the denominator in the integral and to collect the exponential expressions, which can then be integrated. Changing the independent variable τ to $q = 4\tau/A^2$ and using the formula [41] for the three integrations,

$$\int_{-\infty}^{\infty} \mathrm{e}^{-(au^2+2bu+c)}\mathrm{d}u = \sqrt{\frac{\pi}{a}}\mathrm{e}^{(\frac{b^2-ac}{a})} \qquad (\text{for } \; u = x_0, y_0, z_0), \tag{A.11}$$

we can integrate (A.3) and with (A.8) we get the potential $U(x,y,z,\sigma_x,\sigma_y,\sigma_z)$ [6, 37]:

$$U(x,y,z,\sigma_x,\sigma_y,\sigma_z) = \frac{1}{4\pi\epsilon_0}\frac{Ne}{\sqrt{\pi}}\int_0^\infty \frac{\exp\left(-\frac{x^2}{2\sigma_x^2+q}-\frac{y^2}{2\sigma_y^2+q}-\frac{z^2}{2\sigma_z^2+q}\right)}{\sqrt{(2\sigma_x^2+q)(2\sigma_y^2+q)(2\sigma_z^2+q)}}\mathrm{d}q. \tag{A.12}$$

Since we are interested in the transverse fields, we can work with the two-dimensional potential (Appendix A):

$$U(x,y,\sigma_x,\sigma_y) = \frac{ne}{4\pi\epsilon_0}\int_0^\infty \frac{\exp\left(-\frac{x^2}{2\sigma_x^2+q}-\frac{y^2}{2\sigma_y^2+q}\right)}{\sqrt{(2\sigma_x^2+q)(2\sigma_y^2+q)}}\mathrm{d}q, \tag{A.13}$$

where n is the line density of particles in the beam, e the elementary charge and ϵ_0 the electrostatic constant. In this case we do not yet make any assumptions on the longitudinal distribution.

B Appendix B

For the one-dimensional case, we write the betatron motion of a single particle as a simple harmonic oscillator and use the 'smooth approximation':

(B.1)

$$r = R\ \cos(\Phi) \tag{B.2}$$

and its derivative:

$$r' = -\frac{R}{\beta}\ \sin(\Phi). \tag{B.3}$$

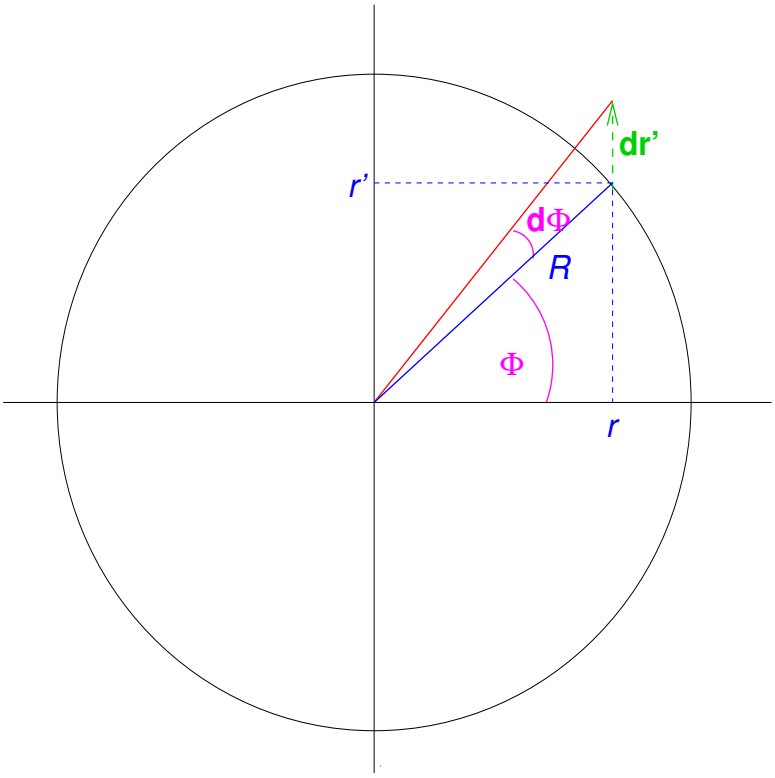

Fig. B.1: Phase space before and after the beam–beam kick. Change of phase $\mathrm{d}\Phi$

After a small kick from the beam–beam interaction the phase Φ will be shifted and we can calculate $\mathrm{d}\Phi$, which is the instantaneous tune change ΔQ_i times 2π (Fig. B.1). We have [36, 39]

$$2\pi\Delta Q_\mathrm{i} \ = \ -\frac{\mathrm{d}r' \cdot \cos(\Phi) \cdot \beta}{R}. \tag{B.4}$$

The deflection $\mathrm{d}r'$ we have calculated in (14):

$$\mathrm{d}r'(r) = -\frac{2Nr_0}{\gamma r}\left[1 - \exp\left(-\frac{r^2}{2\sigma^2}\right)\right] \tag{B.5}$$

and linearized for small amplitudes r it becomes (see Eq. (16))

$$\delta r'|_{r\to 0} \ = \ -\frac{Nr_0 \cdot r}{\gamma\sigma^2} \ = \ -\frac{Nr_0 \cdot R\cos(\Phi)}{\gamma\sigma^2}, \tag{B.6}$$

$$2\pi\Delta Q_\mathrm{i} \ = \ -\frac{Nr_0 \cdot R\cos(\Phi)}{\gamma\sigma^2} \ \cdot \ \frac{\cos(\Phi)\beta}{R}, \tag{B.7}$$

$$\Delta Q_{\rm i} \;=\; -\frac{N r_0 \beta}{2\pi\gamma\sigma^2} \;\cdot\; \cos^2(\Phi). \tag{B.8}$$

After averaging Φ from 0 to 2π:

$$\Delta Q \;=\; \frac{1}{2\pi}\int_0^{2\pi} \Delta Q_{\rm i} {\rm d}\Phi \tag{B.9}$$

we get the linear beam–beam tune shift:

$$\Delta Q \;=\; \xi \;=\; -\frac{N r_0 \beta}{4\pi\gamma\sigma^2}. \tag{B.10}$$

For the non-linear tune shift we must not linearize the beam–beam force and get for the instantaneous tune shift:

$$\Delta Q_{\rm i,nl} \;=\; -\frac{N r_0 \beta}{\pi\gamma} \;\cdot\; \frac{1-{\rm e}^{-\frac{R^2}{2\sigma^2}\cos^2(\Phi)}}{R^2}. \tag{B.11}$$

To perform the integral, we first substitute the $\cos^2(\Phi)$ term in the exponential by the expression

$$\cos^2(\Phi) \;=\; \frac{1}{2}(1+\cos(2\Phi)) \tag{B.12}$$

and then perform the integral using

$$\frac{1}{\pi}\int_0^{\pi} {\rm e}^{x\,\cos(\Phi)} {\rm d}\Phi = I_0(x), \tag{B.13}$$

where $I_0(x)$ is the modified Bessel function, and get the formula for the non-linear detuning with the amplitude J:

$$\Delta Q(J) \;=\; \xi \;\cdot\; \frac{2}{J} \;\cdot\; (1 - I_0(J/2)\cdot {\rm e}^{-J/2}), \tag{B.14}$$

which is $J \;=\; \epsilon\beta/2\sigma^2$ in the usual units. Here ϵ is the particle 'emittance' and not the beam emittance.

C Appendix C

C.1 Classical approach

A standard treatment to assess non-linear perturbations is the s-dependent Hamiltonian and perturbation theory:

$$\mathcal{H} \;=\; \mathcal{H}_0 + \delta(s)\epsilon V, \tag{C.1}$$

where $\mathcal{H}_0$ is the unperturbed part of the Hamiltonian and ϵV describes the perturbation caused at the position s, specified by the δ function. The mathematical treatment is rather involved and in most cases cannot be carried beyond leading order in the perturbation. This can easily lead to wrong conclusions, which can still be found in the literature (e.g. fourth-order resonance cannot be driven by sextupoles) and one must ask the question whether this is the most appropriate tool to deal with this problem. In the case of isolated non-linearities caused by very local beam–beam interactions we favour a map-based approach as promoted by Dragt [42, 43] and described in detail by Forest [44].

C.2 Map-based approach using Lie transforms and invariant

In this approach the ring is represented by a finite sequence of maps, which describe the individual elements. Possible representations of these maps are Taylor maps and Lie maps [38].

In this study we shall use the Lie maps which are always symplectic and other advantages will become obvious [47]. This technique allows to derive invariants of the motion in a straightforward way; in particular, the extension of the results to multiple beam–beam interactions becomes an easy task.

To answer the initial question, this is particularly relevant since we want to investigate the effect of the number of interaction points and the relative phase advance on the beam dynamics.

In the first part we derive the formulae for a single interaction point and later extend the method to multiple beam–beam interactions.

C.2.1 Single interaction point

The derivation for a single interaction point can be found in the literature (see a particularly nice derivation by Chao [38]).

In this simplest case of one beam–beam interaction we can factorize the machine into a linear transfer map $e^{:f_2:}$ and the beam–beam interaction $e^{:F:}$, i.e.

$$e^{:f_2:} \;\cdot\; e^{:F:} \;=\; e^{:h:} \tag{C.2}$$

with

$$f_2 \;=\; -\frac{\mu}{2}\left(\frac{x^2}{\beta} + \beta p_x^2\right), \tag{C.3}$$

where μ is the overall phase, i.e. the tune Q multiplied by 2π, and β is the β-function at the interaction point. The function $F(x)$ corresponds to the beam–beam potential[1]

$$F(x) = \int_0^x \mathrm{d}x' f(x'). \tag{C.4}$$

For a Gaussian beam we use for $f(x)$ the well-known expression for round beams:

$$f(x) = \frac{2Nr_0}{\gamma x}\left(1 - \mathrm{e}^{\frac{-x^2}{2\sigma^2}}\right). \tag{C.5}$$

[1] For a discussion of the Lie representation as a generalized kick map, see [38].

Here N is the number of particles per bunch, r_0 the classical particle radius, γ the relativistic parameter and σ the transverse beam size.

For the analysis we examine the invariant h which determines the one-turn map (OTM) written as a Lie transformation $e^{:h:}$. The invariant h is the effective Hamiltonian for this problem.

As usual we transform to action and angle variables A and Φ, related to the variables x and p_x through the transformations

$$x = \sqrt{2A\beta}\sin(\Phi), \quad p_x = \sqrt{\frac{2A}{\beta}}\cos(\Phi). \tag{C.6}$$

With this transformation we get a simple representation for the linear transfer map f_2:

$$f_2 = -\mu A. \tag{C.7}$$

The function $F(x)$ we write as Fourier series:

$$F(x) \Rightarrow \sum_{n=-\infty}^{\infty} c_n(A)\mathrm{e}^{\mathrm{i}n\Phi} \tag{C.8}$$

with the coefficients $c_n(A)$:

$$c_n(A) \;=\; \frac{1}{2\pi}\int_0^{2\pi} \mathrm{e}^{-\mathrm{i}n\Phi}F(x)\mathrm{d}\Phi. \tag{C.9}$$

For the evaluation of (C.9), see [38]. We take some useful properties of Lie operators (see any textbook, e.g. [38, 44]):

$$:f_2:g(A) = 0, \qquad :f_2:\mathrm{e}^{\mathrm{i}n\Phi} = \mathrm{i}n\mu\mathrm{e}^{\mathrm{i}n\Phi}, \qquad g(:f_2:)\mathrm{e}^{\mathrm{i}n\Phi} = g(\mathrm{i}n\mu)\mathrm{e}^{\mathrm{i}n\Phi} \tag{C.10}$$

and the CBH formula for the concatenation of the maps (see any textbook, e.g. [38, 44]):

$$\mathrm{e}^{:f_2:}\,\mathrm{e}^{:F:} \;=\; \mathrm{e}^{:h:} \;=\; \exp\left[:f_2 + \left(\frac{:f_2:}{1-\mathrm{e}^{-:f_2:}}\right)F + \mathcal{O}(F^2):\right], \tag{C.11}$$

which gives immediately for h

$$h = -\mu A + \sum_n c_n(A)\frac{\mathrm{i}n\mu}{1-\mathrm{e}^{-\mathrm{i}n\mu}}\mathrm{e}^{\mathrm{i}n\Phi}$$

$$\text{and} \quad h = -\mu A + \sum_n c_n(A)\frac{n\mu}{2\sin(\frac{n\mu}{2})}\mathrm{e}^{(\mathrm{i}n\Phi+\mathrm{i}\frac{n\mu}{2})}. \tag{C.12}$$

Away from resonances, a normal-form transformation gives

$$h \;=\; -\mu A + c_0(A) \;= \text{const}. \tag{C.13}$$

On resonance, i.e. for the condition

$$Q = \frac{p}{n} = \frac{\mu}{2\pi} \tag{C.14}$$

and, with $c_n \;\neq\; 0$, we have

$$\sin\left(\frac{n\pi p}{n}\right) = \sin(p\pi) \equiv 0 \quad \text{for all integers} \quad p$$

and the invariant h diverges. This is a well-known result and not surprising.

C.2.2 Non-linear beam–beam tune shift

Having derived the effective Hamiltonian,

$$h \;=\; -\mu A + c_0(A) \;= \text{const.}, \tag{C.15}$$

we can now easily write an expression for the non-linear beam–beam tune shift derived earlier:

$$\Delta Q \;=\; \frac{\mathrm{d}c_0(A)}{\mathrm{d}A}. \tag{C.16}$$

Using the force for a round Gaussian beam and action-angle variables, we write the beam–beam potential $F(x)$ as

$$F(x) = \frac{Nr_0}{\gamma}\int_0^{A\beta/2\sigma^2}(1-\mathrm{e}^{-2\alpha\sin^2(\Phi)})\frac{\mathrm{d}\alpha}{\alpha}. \tag{C.17}$$

The coefficients $c_n(A)$ become

$$c_n(A) = \frac{Nr_0}{\gamma}\int_0^{A\beta/2\sigma^2}\frac{\mathrm{d}\alpha}{\alpha}\frac{1}{2\pi}\int_0^{2\pi}\mathrm{d}\Phi\mathrm{e}^{-in\Phi}(1-\mathrm{e}^{-2\alpha\sin^2(\Phi)}). \tag{C.18}$$

With the coefficient $c_0(A)$ we get for the tune shift as a function of the amplitude:

$$\Delta Q \;=\; \frac{1}{2\pi}\frac{Nr_0}{\gamma}\frac{\mathrm{d}}{\mathrm{d}A}\int_0^{A\beta/2\sigma^2}\frac{\mathrm{d}\alpha}{\alpha}(1-\mathrm{e}^{-\alpha}I_0(\alpha)) \tag{C.19}$$

$$= \frac{1}{2\pi}\frac{Nr_0}{\gamma A}(1-I_0(A\beta/2\sigma^2)\cdot\mathrm{e}^{-A\beta/2\sigma^2}), \tag{C.20}$$

which, for $J = A\beta/\sigma^2$, is the result we obtained earlier.

C.2.3 Two interaction points

To study two interaction points we use a configuration as shown in Fig. C.1 and extend the treatment of a single beam–beam interaction in [45] to any number of beam–beam interactions. Following the LHC conventions we label the interaction points IP1 and IP5. The phase advance between IP1 and IP5 is μ_1, from IP5 to IP1 it is μ_2 and the overall phase advance for one turn is $\mu \;=\; \mu_1 + \mu_2$.

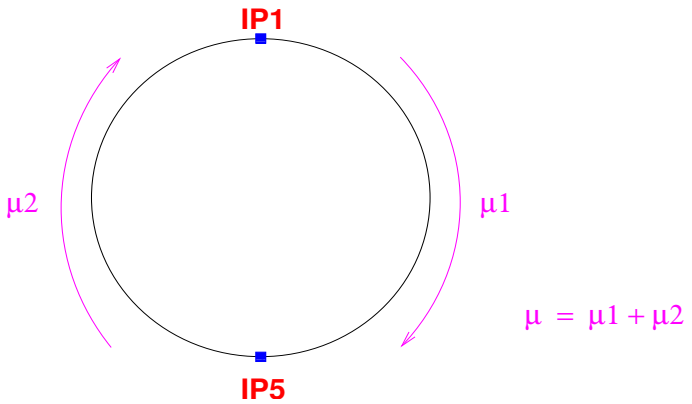

Fig. C.1: Two collision points with unequal phase advance

For the computation we have now two transfers f_2^1, f_2^2 and two beam–beam kicks F^1, F^2, assuming the first interaction point (IP5) at μ_1 and the second (IP1) at μ [46]. The one-turn map with the four transforms is then

$$= \quad \mathrm{e}^{:f_2^1:}\, \mathrm{e}^{:F^1:}\, \mathrm{e}^{:f_2^2:}\, \mathrm{e}^{:F^2:} \;=\; \mathrm{e}^{:h_2:}. \tag{C.21}$$

This we can easily re-write using the properties of Lie operators as

$$\begin{aligned}
&= \quad \mathrm{e}^{:f_2^1:}\, \mathrm{e}^{:F^1:}\, \mathrm{e}^{-:f_2^1:}\, \mathrm{e}^{:f_2^1:}\, \mathrm{e}^{:f_2^2:}\, \mathrm{e}^{:F^2:} \;=\; \mathrm{e}^{:h_2:} \\
&= \quad \mathrm{e}^{:f_2^1:}\, \mathrm{e}^{:F^1:}\, \mathrm{e}^{-:f_2^1:}\, \mathrm{e}^{:f_2:}\, \mathrm{e}^{:F^2:}\, \mathrm{e}^{-:f_2:}\, \mathrm{e}^{:f_2:} \;=\; \mathrm{e}^{:h_2:} \\
&= \quad \mathrm{e}^{:\mathrm{e}^{-:f_2^1:}F^1:}\, \mathrm{e}^{:\mathrm{e}^{-:f_2:}F^2:}\, \mathrm{e}^{:f_2:} \;=\; \mathrm{e}^{:h_2:}.
\end{aligned}$$

Assuming now the simplification

$$f_2 \;=\; -\,\mu A, \quad f_2^1 \;=\; -\,\mu_1 A \;\text{ and }\; f_2^2 \;=\; -\,\mu_2 A \tag{C.22}$$

and, remembering that $g(:\, f_2 \,:)\mathrm{e}^{\mathrm{i}n\Phi} = g(\mathrm{i}n\mu)\mathrm{e}^{\mathrm{i}n\Phi}$, we have

$$\mathrm{e}^{:f_2^1:}\mathrm{e}^{\mathrm{i}n\Phi} \;=\; \mathrm{e}^{\mathrm{i}n\mu_1}\mathrm{e}^{\mathrm{i}n\Phi} \;=\; \mathrm{e}^{\mathrm{i}n(\mu_1+\Phi)} \tag{C.23}$$

and we find that the Lie transforms of the perturbations are phase shifted (see e.g. [44]). Therefore,

$$\mathrm{e}^{:\mathrm{e}^{-:f_2^1:}F^1:}\, \mathrm{e}^{:\mathrm{e}^{-:f_2:}F^2:}\, \mathrm{e}^{:f_2:} \;=\; \mathrm{e}^{:h_2:} \tag{C.24}$$

becomes simpler with substitutions of $\Phi_1 \;\rightarrow\; \Phi + \mu_1$ and $\Phi \;\rightarrow\; \Phi + \mu$ in the functions G^1 and G:

$$\mathrm{e}^{:G^1(\Phi_1):}\mathrm{e}^{:G(\Phi):}\mathrm{e}^{:f_2:} \;\;\Rightarrow\;\; \mathrm{e}^{:G^1(\Phi_1)+G(\Phi):}\mathrm{e}^{:f_2:} \tag{C.25}$$

This reflects the phase-shifted distortions and we get for h_2

$$h_2 = -\mu A + \sum_{n=-\infty}^{\infty} \frac{n\mu c_n(A)}{2\sin(n\frac{\mu}{2})} \left[\mathrm{e}^{-\mathrm{i}n(\Phi+\mu/2+\mu_1)} + \mathrm{e}^{-\mathrm{i}n(\Phi+\mu/2)}\right] \tag{C.26}$$

or, re-written,[2]:

$$h_2 = -\mu A + 2c_0(A) + \underbrace{\sum_{n=2}^{\infty} \frac{2n\mu c_n(A)}{\sin(n\frac{\mu}{2})} \cos\left[n(\Phi + \frac{\mu}{2} + \frac{\mu_1}{2})\right] \cos(n\frac{\mu_1}{2})}_{\text{interesting part}}. \tag{C.27}$$

Note well, because

$$\mathrm{e}^{:F(\Phi):}\mathrm{e}^{:f_2:} \;\;\rightarrow\;\; \mathrm{e}^{:G^1(\Phi_1)+G(\Phi):}\mathrm{e}^{:f_2:}, \tag{C.28}$$

that the above treatment can be generalized to more interaction points, in particular including long-range interactions.

In practice, Eq. (C.27) is evaluated to a maximum order N, in our case up to order 40. We get

$$h_2 = -\mu A + 2c_0(A) + \underbrace{\sum_{n=2}^{N} \frac{2n\mu c_n(A)}{\sin(n\frac{\mu}{2})} \cos\left[n(\Phi + \frac{\mu}{2} + \frac{\mu_1}{2})\right] \cos(n\frac{\mu_1}{2})}_{\text{interesting part}} \tag{C.29}$$

with N = 40.

[2]For head-on collisions only $c_n(A)$ for even orders in n are non-zero and the sum needs to be done only for even terms

C.2.4 Comparison with numerical model

To test our result, we compare the invariant h to the results of a particle-tracking program [46].

The model we use in the program is rather simple:

- linear transfer between interactions;
- beam–beam kick for round beams;
- compute action $I = \frac{\beta^*}{2\sigma^2}(\frac{x^2}{\beta^*} + p_x^2\beta^*)$;
- compute phase $\Phi = \arctan(\frac{p_x}{x})$;
- compare I with h as a function of the phase Φ.

The evaluation of the invariant (C.12) is done numerically with Mathematica.

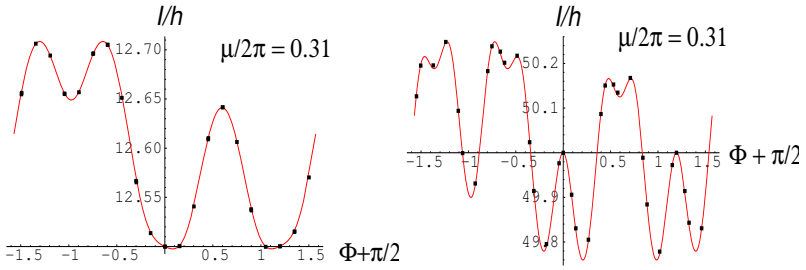

Fig. C.2: Comparison: numerical and analytical models for one interaction point. Shown for $5\sigma_x$ and $10\sigma_x$. Full symbols from numerical model and solid lines from invariant (C.12).

The comparison between the tracking results and the invariant h from the analytical calculation is shown in Fig. C.2 in the (I, Φ) space. Only one interaction point is used in this comparison and the particles are tracked for 1024 turns. The symbols are the results from the tracking and the solid lines are the invariants computed as above. The two figures are computed for amplitudes of 5σ and 10σ. The agreement between the models is excellent. The analytical calculation was again done up to the order $N = 40$. Using a lower number, the analytical model can reproduce the envelope of the tracking results, but not the details.

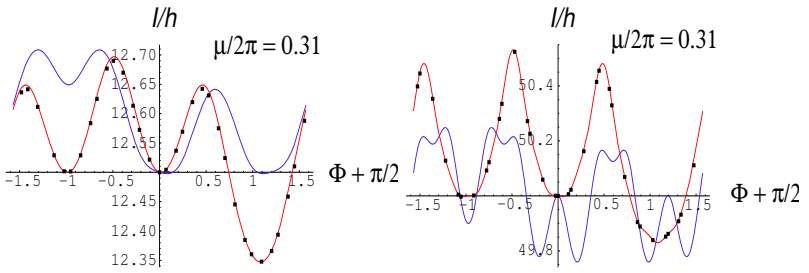

Fig. C.3: Comparison: numerical and analytical models for two interaction points. Shown for $5\sigma_x$ and $10\sigma_x$. Full symbols from numerical model and solid lines from invariant. Shown here are the invariant for one (Eq. (C.12), blue line, not passing through the full symbols) and two (Eq. (C.27), red line, passing through the full symbols) interactions to demonstrate the difference and the agreement with the tracking program.

Another comparison is done in Fig. C.3 for the case of two interaction points. The symbols are again from the simulation and the solid lines from the computation. For comparison, the invariant for a single interaction point is included to demonstrate the difference. Again the agreement is excellent and shows the validity of the results.

C.3 Behaviour near a resonance

To show the behaviour of the system near a resonance, we show the invariant together with the tracking results near the third-order resonance in Fig. C.4.

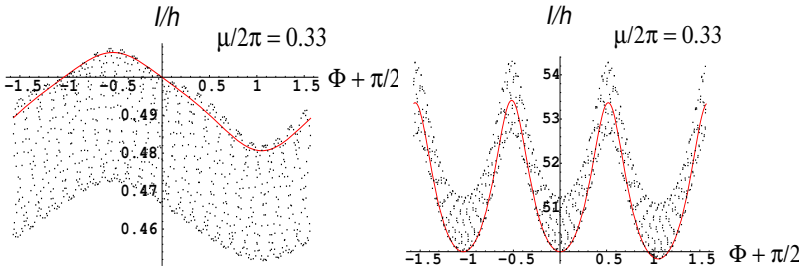

Fig. C.4: Comparison: numerical and analytical models for two interaction points on a resonance (third order)

It is clearly demonstrated that the simulation differs quantitatively from the computed invariant at resonant tunes.